

Optimal design of floating substructures for spar-type wind turbine systems

Ejae Choi, Changwan Han, Hanjong Kim and Seonghun Park*

School of Mechanical Engineering, Pusan National University, Busan, Korea

(Received July 31, 2012, Revised November 4, 2013, Accepted November 6, 2013)

Abstract. The platform and floating structure of spar type offshore wind turbine systems should be designed in order for the 6-DOF motions to be minimized, considering diverse loading environments such as the ocean wave, wind, and current conditions. The objective of this study is to optimally design the platform and substructure of a 3MW spar type wind turbine system with the maximum postural stability in 6-DOF motions as well as the minimum material cost. Therefore, design variables of the platform and substructure were first determined and then optimized by a hydrodynamic analysis. For the hydrodynamic analysis, the body weight of the system was considered, and the ocean wave conditions were quantified to the wave forces using the Morison's equation. Moreover, the minimal number of computation analysis models was generated by the Design of Experiments (DOE), and the design variables of the platform and substructure were finally optimized by using a genetic algorithm with a neural network approximation.

Keywords: floating offshore wind turbines (FOWT); multi-objective optimization; hydrodynamic diffraction analysis; response amplitude operators; artificial neural network; genetic algorithm

1. Introduction

Since wind power generation has relatively high efficiency and market competitiveness among the new renewable energy sources, global technology development and market expansion are now underway in this area (Agarwal and Jain 2003). The early market development of wind power generation mostly focused on wind power generation on land, but these days, offshore wind power generation is receiving much attention as a new alternative due to its advantages, such as steadier and stronger wind with less turbulence, lower area cost, less visual and noise pollution (Leung and Yang 2012, Ma and Patel 2001, Snyder and Kaiser 2009, Tavner 2008). An on-land wind turbine system consists of a rotor that transmits wind energy, a drive train, a power generator and a nacelle where diverse electrical and mechanical devices are installed, as well as a tower that supports the thrust from the blade and the body weight of the structure (Chou *et al.* 1983, Hong *et al.* 2006).

Regarding offshore wind turbine systems which have additional undersea substructures compared with on-land systems, fixed platform concepts, such as tripod, jack-ups, and compliant towers are proposed for shallow waters, while for deep waters, floating platform concepts, such as

*Corresponding author, Professor, E-mail: paks@pusan.ac.kr

tension-leg, semi-submersible, and spar platforms are proposed (Boom *et al.* 1983, Burns 1983, Hua 2011, Moe 2010, Wang and Sweetman 2012).

In the previous study of Robertson and Jonkman, the dynamic responses of two tension-leg platforms (TLP), a semi-submersible platform, a barge platform, and two spar platforms were compared and it was found that the barge platform had the highest dynamic motion while the TLP, semi-submersible, and spar platforms had almost similar dynamic responses (Robertson and Jonkman 2011). Through the numerical and experimental studies, Kurian *et al.* also compared the dynamic motions of classic and truss spar platforms in the frequency domain considering random wave and current forces. The experimental results with a 1:100 scale model were in good agreement with numerical results and showed that higher surge, heave, and pitch motions were observed for the classic spar than the truss spar platform under coupled wave and current forces. They also found that for both types of spar platforms, the dynamic responses in the surge, heave and pitch increased with increasing current velocities under the same random wave condition, while multi-directional waves generated smaller dynamic motions in comparison with long crested waves (Kurian *et al.* 2012a, b, Kurian *et al.* 2012).

Because floating-type wind turbines are not fixed on the seabed, their fatigue life is highly dependent on the dynamic motion stability. Therefore, in order to accurately design the floating substructures of spar-type wind turbines, the exact evaluation of their postural behaviors is necessary and the information on their superstructures as well as variable ocean conditions such as wind, wave, and tidal currents should be considered (Cummins 1962, De Kat and Paulling 1989). However, a limited number of studies have been conducted regarding the hydrodynamic analysis and design of spar platforms for offshore wind turbines. Therefore, this study analyzed the hydrodynamic postural behavior of the spar floating substructure by considering the effect of superstructure on its hydrodynamic motions when it was exposed to an offshore environment, and optimally designed the substructure with high postural stability by using a method that is efficiently combined with a genetic algorithm and an artificial neural network (Chitrapu and Ertekin 1992, Chitrapu *et al.* 1993, Chitrapu 1992).

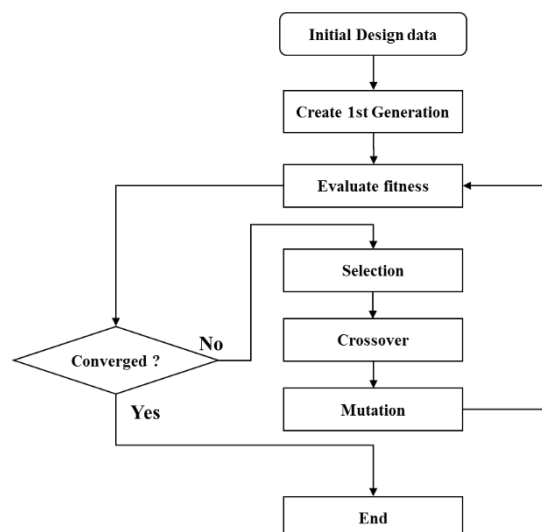


Fig. 1 Schematic diagram of genetic algorithm process

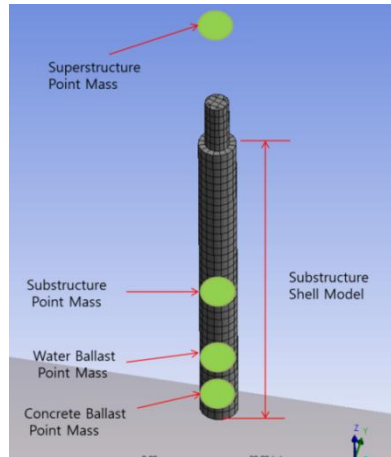


Fig. 2 Finite element 3-D model

2. Finite element 3-Dmodel

For the hydrodynamic analysis, ANSYS AQWA (version 14.0) was used to generate the substructures as the Shell model, and the total number of nodes and elements for the 3D model are 18000 and 22000, respectively, due to the mesh number limitation of the software.

For ANSYS AQWA software we have used in the current study, there is a limitation in the minimum mesh size leading to the limitation of the maximum mesh number that we can generate. Although there is such a limitation, the results of hydrodynamic motions were converged when increasing the number of mesh to the maximum value. The dimensions of meshes were a maximum element size of 3m, a defeaturing tolerance of 1m, and a maximum allowed frequency of 0.294 Hz, the mesh type was Quad mesh (Finnigan *et al.* 1984). The limitation of the mesh size in ANSYS AQWA has also caused shell-type mesh generation with a discrepancy in mesh nodes (i.e., a gap between nodes) for the connecting line of two differently shaped parts (i.e., the upper and lower cylindrical shapes of the current study) due to different mesh sizes, when we try to generate as many meshes as possible for each shape. Although we ignored this discrepancy in mesh nodes in order to increase the mesh number to the maximum value, its effect on the results of this study was negligible because our results were the rigid body motions of the spar substructure (Donley and Spanos 1992, Ertekin and Chitrapu 1988, Faltinsen 1990). The inertia, mass and the center of gravity of the superstructure are shown in Table 1.

Table 1 Superstructure information

Superstructure	Specification
Mass	356500 kg
Center of Mass (X, Y, Z)	(-0.00035932 m, -0.00041835 m, 33.077 m)
Inertia	I _{xx} = 275800000 kg.m ² I _{yy} = 275800000 kg.m ² I _{zz} = 2028000 kg.m ²

A spar-type platform has a structure with relatively high postural stability when exposed to ocean waves since the area touched by the sea surface is smaller than other floating-type substructures, which makes the platform subject to smaller wave loads with a relatively deep draft (Gao and Zou 2008, Hildebrand 1974).

Therefore, for this study, a spar-type platform was selected as the substructure of the offshore wind turbine system. As for the superstructure, a research model was constructed by referring to WinDS3000TM, a 3-MW wind power generator developed by Doosan Heavy Industries and Construction (DHIC) (Huang *et al.* 1982, Jiang and Schellin 1990). The dimensions of the superstructure and 3D Model are shown in Table 2.

Table 2 Dimensions and weights of the 3-D model

Parts	Category	Specification
Nacelle	Weight	120 tons
	Height	3.2 m
Tower	Weight	180 tons
	Height	65 m
	Diameter Top	3 m
	Diameter Bottom	4.5 m
	Thickness Top	0.05 m
	Thickness Bottom	0.1 m
Blade	Weight	31.5 tons
Hub	Weight	25 tons
	Height	65 m
Substructure	Diameter Top	8 m
	Diameter Bottom	8 m
	Thickness Top	0.15 m
	Thickness Bottom	0.23 m

3. Hydrodynamic diffraction analysis

In this study, only the wave loads were considered, because they provide the most significant effect on the postural behavior of offshore structures. Furthermore, the sea water was assumed to be an ideal fluid, non-rotational and incompressible

The maximum wave height and pressure exerted to the structural change in accordance with the wave frequency of 0.011 Hz, which causes the maximum dynamic motion, was selected for this analysis. The offshore environment is shown in Fig. 2, with the XY plane representing the sea surface and the -Z direction indicating gravity. Before conducting the analysis using ANSYS AQWA, the offshore geometry conditions, which assume a deep-sea environment, are shown in Table 3. The seawater depth and width were set to 200 m and 300*300 m², respectively, with a density of 1025 kg/m³. The wave height and range were set to 3m and -180° to 180° (-PI to PI, means all directions), respectively. The number of wave frequency was 20 and wave was given in the X and Y directions (Haug and Fjeld 1996, Kobayashi *et al.* 1987).

As for the wave power that was used in the hydrodynamic diffraction analysis, the wave power exerted to the structure can be calculated by using the Morison Equation (Kim and Yue 1991, Yilmaz and Incecik 1996). The equation is shown below

$$F = \rho C_m V \dot{u} + 0.5 \rho C_d A u |u| \quad (1)$$

where F is the Morison force, ρ is the water density, C_m is the inertia coefficient, C_d is the drag coefficient, V is the volume of the body, A is the reference area, and u is the flow velocity.

The hydrodynamic diffraction analysis model and the static structural analysis model were constructed by using ANSYS Design Modeler, a general-purpose analysis program. First, the static structural analysis was conducted by using a substructure model consisting of a solid body with the purpose of finding out information on the point mass in the Shell model for hydrodynamic diffraction analysis. Second, the information on point mass obtained through the process above was applied to the Shell model, and the hydrodynamic diffraction analysis by ANSYS AQWA led to calculating the pressure and the postural behavior of the offshore structure exposed to such offshore conditions (i.e., wave loads). Finally, the hydrodynamic diffraction analysis results of 9 substructure 3D models produced by the Design of Experiments (design variables, such as the diameter, the height, the weight of the concrete and water ballast) were used as the input of the optimal design with a genetic algorithm in order to obtain the optimal values of the design variables. Fig. 3 shows the flow chart of the hydrodynamic diffraction analysis. Design variable levels and design of experiments (DOE), which results in the generation of 9 analysis models are shown in Tables 4 and 5, respectively.

Table 3 Offshore geometry conditions

Geometry	Specification
Water Depth	200 m
Water Density	1025 kg/m ³
Water Size, X	300 m
Water Size, Y	300 m
Sea Grid Size Factor	15

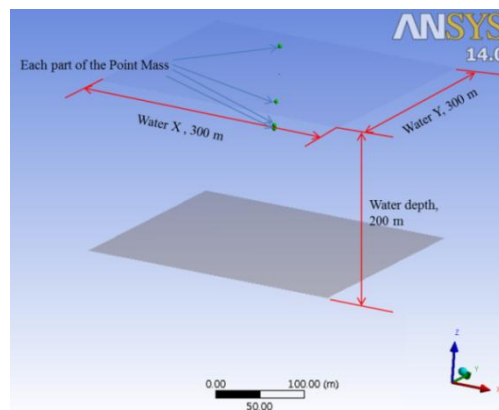


Fig. 3 Offshore environments for hydrodynamic diffraction analysis

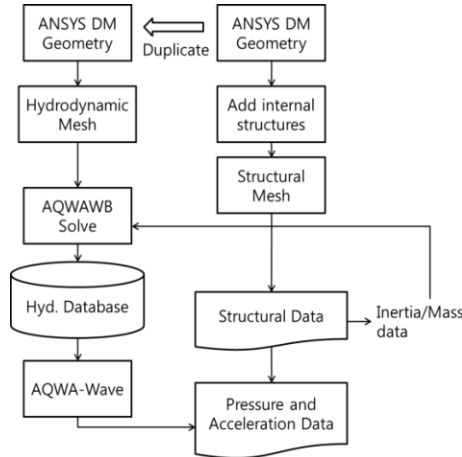


Fig. 4 Hydrodynamic analysis procedure

Table 4 Design variable levels

Height	[m]	Diameter	[m]	Ballast	Concrete[%]	Water[%]
0	65	0	7	0	40	60
1	75	1	9	1	60	40
2	85	2	11	2	80	20

Table 5 Design of experiments (DOE)

	Height	Diameter	Ballast
1	0	0	0
2	0	1	1
3	0	2	2
4	1	0	1
5	1	1	2
6	1	2	0
7	2	0	2
8	2	1	0
9	2	2	1

For the calculation of the ballast weight with concrete and water was computed to locate the platform of every model at the same mean water level by first calculating the weight of the substructure and superstructure and the amount of water displaced by the substructure. To increase the postural stability of the wind turbines, concrete was placed below water in the ballast due to higher density of concrete than water. Furthermore, all the mass information of the substructure, superstructure, concrete and water were inputted into the point mass for the hydrodynamic analysis. Then, the raw material price index of the 9 models was computed (Table 6).

Table 6 Raw material price index of the 9 models generated by DOE

Model	Displacement[m ³]	Total Weight[kg]	Weight of concrete [kg]	Weight of Water [kg]	Cost of Steel [KRW]	Cost of concrete [KRW]	Raw material price index
1	2500.225	2176792	139846	209769	2276924432	14386251	22273467
2	4133.025	2857341	805914	537276	2988778686	82905872	29859357
3	6174.025	3556633	2189304	547326	3720238118	225217728	38353148
4	2884.875	2495888	254894	169929	2610698848	26221500	25633084
5	4768.875	3270150	1265799	316449	3420576900	130215077	34516684
6	7123.875	4063156	1281576	1922364	4250061176	131838102	42595746
7	3269.525	2814983	400027	100006	2944472218	41151527	29022774
8	5404.725	3682959	728522	1092784	3852375114	74944496	38176850
9	8073.725	4569678	2202750	1468500	4779883188	226601011	48667236

4. Analysis results

Response Amplitude Operators (RAOs), which indicate the ratio of output to input amplitude for the resulting harmonic response output from the forced harmonic input, were obtained from the hydrodynamic diffraction analysis by using the hydrostatic analysis results (i.e., 3 by 3 stiffness matrix of the floating offshore structure).

RAOs of displacements and rotations for the first model (Model 1) among 9 models generated by the DOE were shown in Figs. 4 and 5. For all 9 models, the roll (GRX) and pitch (GRY) were symmetrical with regard to the incident wave angle, similarly to the surge (GX) and sway (GY). Maximum GX and GY values ranged from 2.96 to 3.11 m/m for all 9 models, and the heave (GZ) was in the range of 1.01 to 2.60 m/m. Maximum GRX and GRY were ranged from 0.19 to 3.64 °/m with the yaw (GRZ) ranged from 0.078 to 0.85 °/m.

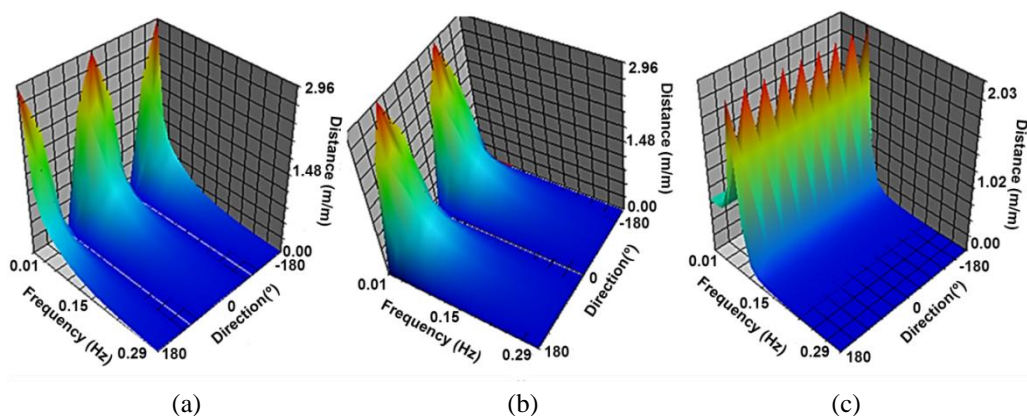


Fig. 5 RAOs of the (a) surge (GX), (b) sway (GY) and (c) heave (GZ) (model 1)

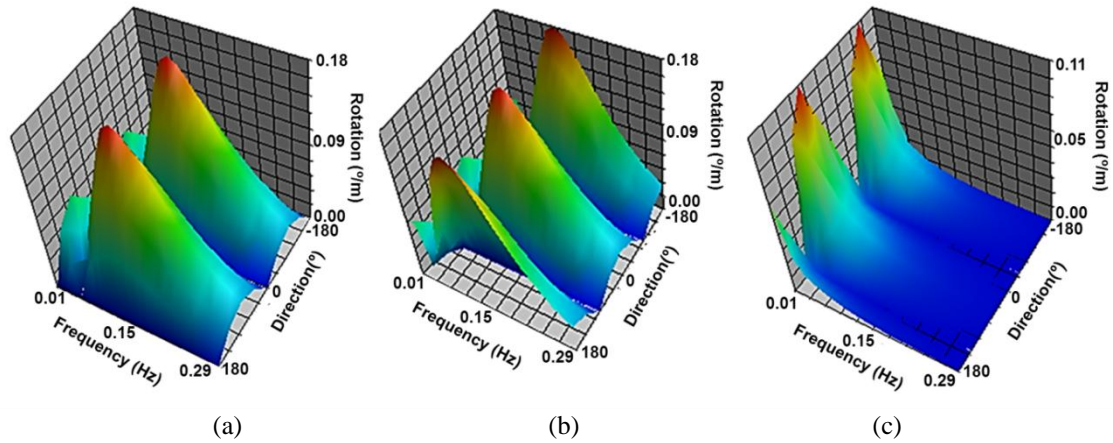


Fig. 6 RAOs of the (a) roll (GRX), (b) pitch (GRY) and (c) yaw (GRZ) (model 1)

In the present study, considering both that the surge and sway motions were not much different and the effect of the yaw on the damage of the offshore structure were not significant compared with the roll and pitch, the roll and pitch were selected as objective postural behavior index for optimizing design variables.

5. Multiple objective optimization

The design variables (i.e. the diameter, the height, the weight of the concrete and water ballast of the substructure) are optimized in terms of the postural behavior stability and raw material price index; the raw material price index is employed in order to easily calculate the total price of the substructure from the substructure weight. The current optimization method is efficiently combined with a genetic algorithm and an artificial neural network as shown in Fig. 6 (Lee *et al.* 2009). Prior to the search for the optimum solution, artificial neural network is first used for approximation of the hydrodynamic analysis results of the 9 finite element models produced by the design of experiments. For the optimization of the design variables, a genetic algorithm is adopted due to the advantage of the search for the global optimum solution to overcome local minimums by jumping over constraint boundaries in the search space. Another advantage in the context of our integrated multi-objective design is that a genetic algorithm works well with experimental data as well as simulated data because a number of parameters change drastically over the range of the design variables for a complicated system with numerous constraints, resulting in a set of optimum candidate solutions rather than a single candidate solution.

In the present study, therefore, for the multi-objective optimization of the three design variables (i.e., height, diameter, concrete ratio), each ideal level of postural stability and material price index is first obtained through their single optimization, and the ideal levels of postural stability (f_1^*) and material price index (f_2^*) are expressed by

$$F^* = \{f_1^*, f_2^*\} \quad (2)$$

Then, to determine weighting factors for multi-objective optimization, aspiration levels of postural stability (\hat{f}_1^k) and material price index (\hat{f}_2^k) are denoted by

$$\hat{F}^k = \{\hat{f}_1^k, \hat{f}_2^k\} \tag{3}$$

where the superscript k denotes the number of adjustments in aspiration levels to find the desired multi-objective optimization solutions. Using these ideal and aspiration levels, two weighting factors regarding postural stability and material price index are defined by differences between ideal levels and aspiration levels as shown below

$$w_1^k = \frac{1}{|f_1^* - \hat{f}_1^k|}, \quad w_2^k = \frac{1}{|f_2^* - \hat{f}_2^k|} \tag{4}$$

The multi-objective optimization function with trade-off between postural stability and material price index is formulated by the equation

$$\begin{aligned} F^k(\mathbf{x}) &= \max\{w_1^k \cdot |f_1^* - f_1(\mathbf{x})|, w_2^k \cdot |f_2^* - f_2(\mathbf{x})|\} \\ &= \max\left\{\frac{|f_1^* - f_1(\mathbf{x})|}{|f_1^* - \hat{f}_1^k|}, \frac{|f_2^* - f_2(\mathbf{x})|}{|f_2^* - \hat{f}_2^k|}\right\} \end{aligned} \tag{5}$$

where \mathbf{x} is the design variables (i.e., height, diameter, concrete ratio) and $f_1(\mathbf{x})$ and $f_2(\mathbf{x})$ are the learning outputs of postural stability and material price index calculated from artificial neural network, respectively. After the hydrodynamic analysis results of the 9 finite element models are given to the learning inputs of the neural network with details shown in Table 7, the learning outputs $f_1(\mathbf{x})$ and $f_2(\mathbf{x})$ are then calculated for the design variables \mathbf{x} with the minimum and maximum ranges of the design variables as constraints as shown in the flow chart of artificial neural network (Fig. 8).

Table 7 Optimization conditions

Category	Value		
Neural network hidden layer	2		
Neural network hidden layer connection	10		
Learning coefficient	0.05		
Convergence ratio	0.02		
Genetic algorithm population	40		
Convergence condition	7 repetitions of the objective value		
Crossover rate	0.4		
Mutation rate	0.005		
Optimization ranges of design variables*	H: 65~85 m	D: 7~11 m	C:40~80%
Digitization numbers of design variables*	H: 160	D: 160	C: 120

*Design variables: height (H), diameter (D), concrete ratio (C)

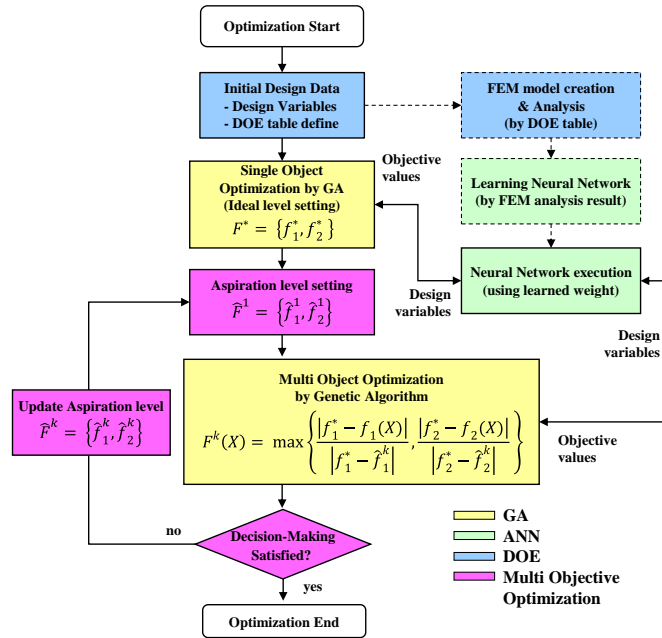


Fig. 7 Schematic diagram of multi-objective optimization

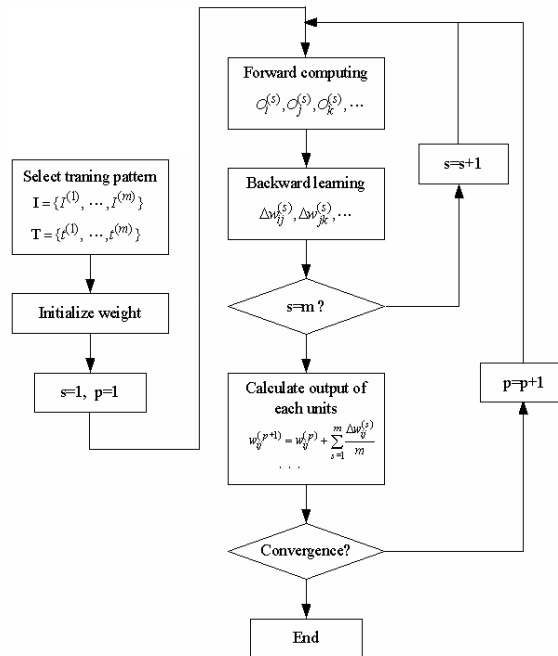


Fig. 8 Flow chart of approximation process with artificial neural network

In the current study, the weighting factors were adjusted k^{th} times by updating the aspiration levels manually (Table 8), and the adjustments were rather focused on the minimization of postural stability between its ideal and current levels (i.e., $f_1^* - f_1(\mathbf{x})$) than that of material price index (i.e., $f_2^* - f_2(\mathbf{x})$).

Finally, the optimal design variable values as well as the concomitant postural behavior and raw material price index values (i.e., the best objective values) were obtained after 109th generation, as shown below.

- Best objective value [RGX]: 0.193°/m
- Best objective value [Raw material price index]: 2.356E+07
- Optimized design variables: 69.25 m (Height), 7.0 m (Diameter), 40.0% (Concrete ratio)
- End generation: 109th generation

The best objective roll value (GRX) was 0.193°/m, which is the roll and pitch of the substructure calculated by the optimization process after being converged (Fig. 9). To prove the accuracy of our optimization process, we performed another hydrodynamic diffraction analysis with the optimized design variable values, and the acquired roll (GRX) value was 0.213°/m which is very close to the objective GRX value (0.193°/m).

Table 8 Multi-objective optimization results through aspiration level updates

k	Aspiration level		Weighting factor		Optimized value		Ideal level	
	Stability	Price index	Stability	Price index	Stability	Price index	Stability	Price index
1	0.300	3.0000E+07	9.09	1.1655E-07	0.246	2.2514E+07		
⋮	⋮	⋮	⋮	⋮	⋮	⋮		
10	0.200	2.2000E+07	100	1.7241E-06	0.219	2.2316E+07		
11	0.191	2.4000E+07	1000	3.8760E-07	0.197	2.3762E+07	0.19	2.1420E+07
12	0.200	2.3000E+07	100	6.3291E-07	0.207	2.2347E+07		
13	0.191	2.2000E+07	1000	1.7241E-06	0.203	2.2348E+07		
14	0.195	2.1500E+07	200	1.2500E-05	0.193	2.3560E+07		

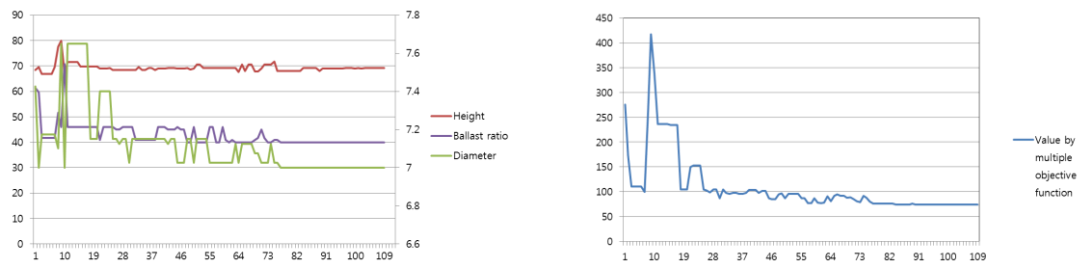


Fig. 9 Convergence of designvariables and multi-objective function during optimization

6. Conclusions

The current study examined design optimization in the overall shape of the substructure for spar-type wind turbines by combining a genetic algorithm with a neural network to approximate the hydrodynamic analysis results of the substructure design models. The optimal design values of the height, diameter, ballastweight to simultaneously satisfy both the postural stability and low material cost were proposed. The accuracy in our optimization process was also proved by comparing the roll calculated by the optimization process with the value computed from hydrodynamic analysis using the optimized design variables. These results suggest that the combination of diverse methodologies used in the present study works well to efficiently and accurately solve our integrated multi-objective design problem, and moreover can provide important design guidelines of spar type floating platforms and substructures.

Acknowledgements

This research was supported by the New & Renewable Energy of the Korea Institute of Energy Technology Evaluation and Planning (KETEP) grant funded by the Korea government Ministry of Trade, Industry and Energy (No. 20113020020010-11-1-000) and by Leading Foreign Research Institute Recruitment Program through the National Research Foundation of Korea (NRF) grant funded by the Ministry of Science, ICT & Future Planning (No.2013044133).

References

- Agarwal, A. and Jain, A. (2003), "Dynamic behavior of offshore spar platforms under regular sea waves", *Ocean Eng.*, **30**(4), 487-516.
- Boom, W.D., Pinkster, J. and Tan, S. (1983), "Motion and tether force prediction for a deepwater tension leg platform", *Proceedings of the Offshore Technology Conference*.
- Burns, G.E. (1983), "Calculating viscous drift of a tension leg platform", *Proceedings of the 2nd International Offshore Mechanics and Arctic Engineering Symposium*, Houston, Texas, February.
- Chitrapu, A. and Ertekin, R. (1992), *Effect of nonlinear drag forces on the low-and high-frequency response of floating platforms*.
- Chitrapu, A., Ertekin, R. and Paulling, J. (1993), "Viscous drift forces in regular and irregular waves", *Ocean Eng.*, **20**(1), 33-55.
- Chitrapu, S. (1992), *Nonlinear forces and response of floating platforms in regular and random waves*.
- Chou, F.S., Ghosh, S. and Huang, E.W. (1983), *Conceptual design process of a tension leg platform*, Society of Naval Architects and Marine Engineers.
- Cummins, W. (1962), *The impulse response function and ship motions*, DTIC Document.
- De Kat, J.O. and Paulling, J.R. (1989), "The simulation of ship motions and capsizing in severe seas", *T. Soc. Naval Archit. Marine Engineers*, **97**, 139-168.
- Donley, M. and Spanos, P. (1992), "Stochastic response of a tension leg platform to viscous and potential drift forces", *Proceedings of the 11th Int. Offshore Mech. and Arctic Engineering Conf*, New York, NY.
- Ertekin, R. and Chitrapu, A. (1988), "Wave-and current-induced viscous drift forces on floating platforms", *Offshore Engineering* (Eds. Cameiro, F.L.L.B., Ferrante, A.J. and Batista, R.C.), **6**, 615-629.
- Faltinsen, O. (1990), "Wave loads on offshore structures", *Annu. Rev. Fluid Mech.*, **22**(1), 35-56.
- Finnigan, T., Petruskas, C. and Botelho, D. (1984), "Time-domain model for TLP surge response in extreme sea states", *Proceedings of the Offshore Technology Conference*.

- Gao, Z.I. and Zou, Z.J. (2008), "A three-dimensional desingularized high order panel method based on NURBS", *J. Hydrodynamics, Ser. B*, **20**(2), 137-146.
- Haug, A. and Fjeld, S. (1996), "A floating concrete platform hull made of lightweight aggregate concrete", *Eng. Struct.*, **18**(11), 831-836.
- Hildebrand, F. (1974), *Introduction to numerical analysis, international series in pure and applied mathematics*, McGraw-Hill, New York.
- Hong, H., Park, J., Bang, J., Ryu, J. and Kim, D. (2006), "Research for 2 MW wind turbine tower shell design optimization", *J Korean SOC New & Renew Energ*, 19-26.
- Hua, J. (2011), "A floating platform of concrete for offshore wind turbine", *J. Renew. Sust. Energ. Rev.*, **3**(6), 063103-063113.
- Huang, X., Hoff, J. and Naess, A. (1982), "Loads and motions measured on a semisubmersible having a large permanent list angle", *Norwegian Maritime Res.*, **10**(2), 24-33.
- Jiang, T. and Schellin, T. (1990), "Motion prediction of a single-point moored tanker subjected to current, wind and waves", *J. Offshore Mech. Arct.*, **112**(2), 83-90.
- Kim, M. and Yue, D. (1991), *Sum and difference -frequency wave loads on a body in unidirectional Gaussian seas*.
- Kobayashi, M., Shimada, K. and Fujihira, T. (1987), "Study on dynamic responses of a TLP in waves", *J. Offshore Mech. Arct.*, **109**(1), 61-66.
- Kurian, V., Ng, C. and Liew, M. (2012a), "Experimental investigation on dynamic responses of spar platforms subjected to multi-directional waves", *Proceedings of the Business Engineering and Industrial Applications Colloquium (BEIAC)*, 2012 IEEE.
- Kurian, V., Ng, C. and Liew, M. (2012b), "Numerical investigation on dynamic responses of classic spar platforms: Long crested waves vs. short crested waves", *Proceedings of the Humanities, Science and Engineering (CHUSER)*, 2012 IEEE Colloquium on.
- Kurian, V.J., Tuhaijan, S.N.A. and Liew, M.S. (2012), "Dynamic responses of spar acted upon by random wave and current", *Proceedings of the Business Engineering and Industrial Applications Colloquium (BEIAC)*, 2012 IEEE, 7-8 April.
- Lee, J.H., Kim, M., Park, S., Kang, J.K., and Lee, S. (2009), "Optimum bar-feeder support positions of a miniature high speed spindle system by genetic algorithm", *Precis Eng.*, **26**, 99-107.
- Leung, D.Y. and Yang, Y. (2012), "Wind energy development and its environmental impact: a review", *Renew. Sust. Energ. Rev.*, **16**(1), 1031-1039.
- Ma, Q. and Patel, M. (2001), "On the non-linear forces acting on a floating spar platform in ocean waves", *Appl. Ocean Res.*, **23**(1), 29-40.
- Moe. (2010), "Floating turbine captures wind energy in deep-water environment", *Weld J.*, **89**(5), 54-58.
- Robertson, A.N. and Jonkman, J.M. (2011), *Loads analysis of several offshore floating wind turbine concepts*, National Renewable Energy Laboratory, US Department of Energy, Office of Energy Efficiency and Renewable Energy.
- Snyder, B. and Kaiser, M. J. (2009), "Ecological and economic cost-benefit analysis of offshore wind energy", *Renew. Energ.*, **34**(6), 1567-1578.
- Tavner, P. (2008), "Wind power as a clean-energy contributor", *Energy Policy*, **36**(12), 4397-4400.
- Wang, L. and Sweetman, B. (2012), "Simulation of large-amplitude motion of floating wind turbines using conservation of momentum", *Ocean Eng.*, **42**, 155-164.
- Yilmaz, O. and Incecik, A. (1996), "Hydrodynamic design of moored floating platforms", *Mar. Struct.*, **9**(5), 545-575.